

brational frequencies from one-photon spectroscopy, and new information can be expected from two-photon spectroscopy. The b_2 vibrations have been assigned by the following procedure: As the ground electronic state frequencies for ν_8 and ν_9 vibrations are known from the literature,^{16,17} the 8_1^0 (27 283.2 cm^{-1}) and the 9_1^0 hot bands (27 830.0 cm^{-1}) can be readily assigned in the two-photon spectrum. In Figure 5a,b the relevant parts of the two-photon spectrum are shown. Both the 8_1^0 as well as the 9_1^0 bands are located on a background resulting from the wings of the rotational envelopes of the strong $4_0^1 1_1^0$ (27 328.0 cm^{-1}) and the 4_1^0 (27 888.7 cm^{-1}) transition, respectively. Even though the details of the rotational structure of the 8_1^0 and 9_1^0 bands cannot be resolved, it is seen that they differ from that of the a_1 , a_2 , and b_1 vibrational bands. Striking features are the sharp cutoff at the blue edge of the band, two small peaks at the red side of the band (marked with arrows), and the lack of a dominating R branch. No changes in the rotational contour of the nontotally symmetric A_2 two-photon transition are expected when polarization is changed from linear to circular, and indeed, this is detected for these assigned bands. The rotational origins of the hot bands at 27 283.2 cm^{-1} (8_1^0) and 27 830.0 cm^{-1} (9_1^0) are found from a comparison with the infrared¹⁶ and Raman^{16,17} data. They are located at the sharp cutoff of the bands, as indicated in Figure 5.

Weak vibronic bands with similar rotational envelopes are found in the cold-band two-photon spectrum at 29 245.4 cm^{-1} (8_0^0) and 28 723.6 cm^{-1} (9_0^0). From this, we find a value of 871.3 cm^{-1} for the ν_8 and a value of 349.5 cm^{-1} for the ν_9 vibrational frequencies in the 1B_1 excited electronic state in reasonable agreement with the frequencies calculated by Rolfe et al.²⁰

Summary and Conclusion

In this work, the low-pressure gas-phase two-photon excitation spectrum of the photodissociating molecule difluorodiazirine, F_2CN_2 , was measured under Doppler-limited resolution. On the basis of a detailed analysis of the hot-band region and the analysis of the gross features of the rotational envelopes, nearly all observed transitions have been assigned. In particular, b_1 vibrational bands can be unambiguously assigned by their striking polarization behavior in linearly vs circularly polarized light.

The bands with a_1 , b_1 , and b_2 vibrational symmetry were discussed in detail. For some of these bands, revised or new assignments are made. The ν_5 vibration, the only vibration of a_2

symmetry, was not discussed in detail; its previous assignment was corroborated by the two-photon spectroscopy of this work.

Finally, a complete set of vibrational frequencies in the excited electronic (1B_1) state of difluorodiazirine is obtained. In particular, three previously unknown vibrational frequencies ν_6 (1317.7 cm^{-1}), ν_8 (871.3 cm^{-1}), and ν_9 (349.5 cm^{-1}) are found, and new frequency values for ν_2 (785.1 cm^{-1}) and ν_7 (472.2 cm^{-1}) are evaluated, which differ considerably from previous values (865.7 cm^{-1} , 332.9 cm^{-1}) found from a one-photon analysis.^{8,10,11}

The ground-state and the excited electronic state frequencies found in this work are listed in Table I together with theoretical values and with previously found values from one-photon and Raman measurements.

It is interesting to note that there is nearly no frequency change δ of ν_4 ($\delta = 15.8 \text{ cm}^{-1}$) and ν_7 ($\delta = -7.0 \text{ cm}^{-1}$) from the ground to the excited electronic state. ν_4 is a symmetric and ν_7 is an asymmetric CF bond deformation mode. In addition, the frequency of the asymmetric CF stretching mode ν_6 ($\delta = 69.1 \text{ cm}^{-1}$) increases slightly in the excited electronic state.

By contrast, the vibrations ν_2 and ν_3 leading to a symmetric stretching not only of the CF bond but also of the CN bond (ν_3) and additionally the NN bond (ν_2) display a strong (ν_2) ($\delta = -497.3 \text{ cm}^{-1}$) and a moderate (ν_3) ($\delta = -162.0 \text{ cm}^{-1}$) decrease of frequency in the excited state. A similar behavior is observed for the ν_8 vibration ($\delta = -219.6 \text{ cm}^{-1}$), which is an asymmetric CN stretching mode.

From these results, it is concluded that there is a tightening of the CF bonds and a loosening of the CN bonds in the electronic excited state. This result is in line with the dissociation pathway of F_2CN_2 leading to CF_2 and N_2 and may be further confirmed by a detailed analysis of the rotational structure of the various vibronic bands yielding accurate rotational constants. Here, the application of Doppler-free techniques (like Doppler-free two-photon absorption) might be helpful and will be accomplished in forthcoming experiments in this laboratory.

Acknowledgment. We are indebted to Prof. E. W. Schlag for his permanent interest and grateful to Dr. E. Riedle for helpful discussions and experimental assistance. Financial support from the Deutsche Forschungsgemeinschaft is gratefully acknowledged. H.S. thanks the Hanns-Seidel-Stiftung for a "Graduierten Stipendium".

Registry No. Difluorodiazirine, 693-85-6.

Ammonia Activation by V^+ : Electronic and Translational Energy Dependence

D. E. Clemmer, L. S. Sunderlin, and P. B. Armentrout*[†]

Department of Chemistry, University of Utah, Salt Lake City, Utah 84112 (Received: May 16, 1989)

The reaction of V^+ with ammonia is studied as a function of translational energy in a guided ion beam tandem mass spectrometer. The effect of electronic energy is also probed by varying the conditions for forming V^+ . The a^3F state of V^+ is found to be substantially more reactive than the a^5D ground and a^5F first excited states. The results indicate that reaction occurs primarily through a triplet $H-V^+-NH_2$ intermediate. The reactivities of the different electronic states of V^+ can be explained by using molecular orbital and spin conservation concepts. The thresholds for the cross sections of the endothermic reactions are interpreted to give the 298 K bond energies of $D^0(V^+-NH_2) = 3.18 \pm 0.10$, $D^0(V^+-NH) = 4.30 \pm 0.16$, and $D^0(V^+-N) = 4.65 \pm 0.06$, all in electronvolts. The large bond strengths of V^+-NH_2 and V^+-NH indicate that the lone pair electrons on the nitrogen atom are involved in the metal-ligand bond.

Introduction

The study of the reactions of atomic transition metal ions with H_2 and hydrocarbons has provided insight into the activation of hydrocarbon bonds.^{1,2} State-specific studies of the periodic trends in this chemistry have provided a more complete understanding

of the electronic requirements for such H-H, C-H, and C-C bond activations.¹ Here, we extend this work to examine the activation of the N-H bonds of ammonia. The activation of N-H bonds

[†]NSF Presidential Young Investigator, 1984-1989; Alfred P. Sloan Fellow; Camille and Henry Dreyfus Teacher-Scholar, 1988-1993.

(1) Armentrout, P. B. In *Gas Phase Inorganic Chemistry*; Russell, D. H., Ed.; Plenum: New York, 1989; pp 1-42. Armentrout, P. B.; Beauchamp, J. L. *Acc. Chem. Res.* in press.

(2) Allison, J. *Prog. Inorg. Chem.* **1986**, *34*, 627-676.

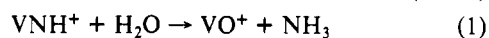
TABLE I: Heats of Formation and Bond Strengths for NH_n Species (298 K)^a

| neutral | $\Delta_f H^\circ$, eV | bond | D° , eV |
|-----------------|---|--------------------|--|
| H | 2.259 (0.0001) | N-H | 3.45 ₅ (0.01 ₃) |
| N | 4.899 (0.001) | HN-H | 4.00 ₃ (0.01 ₆) |
| NH | 3.70 ₃ (0.01 ₃) ^b | HN-H ₂ | 4.17 ₉ (0.01 ₄) |
| NH ₂ | 1.96 (0.009) ^b | H ₂ N-H | 4.69 ₅ (0.01 ₄) |
| NH ₃ | -0.476 (0.004) | | |

^aAll values except where noted are from ref 15. Uncertainties are in parentheses. ^bDerived from $\Delta_f H^\circ_0$ results for NH and NH₂ in: Anderson, W. R. *J. Phys. Chem.* **1989**, *93*, 530-536.

is of topical interest in both the gas phase^{3,4} and condensed phase.⁵⁻¹¹

The present study reports guided ion beam studies of the reaction of V⁺ with ammonia. Buckner, Gord, and Freiser (BGF) have previously examined this system by using Fourier transform ion cyclotron resonance (FTICR) mass spectrometry.³ They observed the exothermic formation of VNH⁺ as the only reaction at thermal energies. BGF noted that the exothermicity of this reaction means that the V⁺-NH bond strength exceeds $D^\circ(\text{NH}-\text{H}_2)$, which they cited as 4.03 eV. More recent thermochemistry establishes that this limit is actually 4.18 ± 0.01 eV (Table I). BGF also determined an upper limit to this bond energy by observing the exothermic reaction 1. On the basis of $D^\circ(\text{V}^+-\text{O})$



= 5.68 ± 0.17 eV,¹² they report $D^\circ(\text{V}^+-\text{NH}) < 4.34 \pm 0.26$ eV. A more accurate value for $D^\circ(\text{V}^+-\text{O})$ is 5.98 ± 0.10 eV.¹³ When combined with literature thermochemistry,^{14,15} this value leads to the conclusion that $D^\circ(\text{V}^+-\text{NH}) \leq 5.07 \pm 0.10$ eV. BGF conclude that $D^\circ(\text{V}^+-\text{NH}) = 4.38 \pm 0.30$ eV, although the more accurate thermochemistry means that they can only provide the broad limits of $4.17 \text{ eV} < D^\circ(\text{V}^+-\text{NH}) < 5.17 \text{ eV}$.

In this work, we examine the interaction of V⁺ with ammonia over an extended kinetic energy range, such that we study the endothermic as well as the exothermic reactions. This permits a detailed dynamic study of the interaction of V⁺ with ammonia and allows a comprehensive evaluation of the thermochemistry of V⁺-NH_n ($n = 0-2$). In addition, we compare these results with the previous examination by Aristov and Armentrout (AA) of the state-specific reactivity of V⁺ with methane.¹⁶ Because methane is isoelectronic with ammonia (in the sense that the central heavy atom has the same number of valence electrons with the same sp³ hybridization),¹⁷ this study provides an excellent reference point for understanding the present results.

Results of the methane experiment show that electronic energy from excited-state vanadium ions couples efficiently to the reaction coordinates of all product channels. The reactivity of the a³F state was found to be over 2 orders of magnitude greater than that of

TABLE II: V⁺ Beam State Populations

| state | electron confign | energy, ^a eV | % population | | | |
|----------------------|-------------------|----------------------------|---------------------|---------------------|---------------------|----------------------|
| | | | 1950 K ^b | 2200 K ^b | 30 eV | 50 eV |
| a ⁵ D | 3d ⁴ | 0.026 | 84.0 (1.4) | 80.6 (1.4) | 40 ^c | ~0 ^c |
| a ³ F | 4s3d ³ | 0.36 | 15.9 (1.4) | 19.1 (1.3) | | |
| a ³ F | 4s3d ³ | 1.10 | 0.116 (33) | 0.230 (51) | 9 (3) ^c | 5 (2) ^c |
| a ³ P | 3d ⁴ | 1.45 | 0.006 | 0.016 | | |
| a ³ H | 3d ⁴ | 1.57 | 0.012 | 0.031 | | |
| b ³ F | 4s3d ³ | 1.68 | 0.004 | 0.011 | | |
| a ³ P | 4s3d ³ | 1.69 | 0.002 | 0.007 | | |
| a ³ G | 3d ⁴ | 1.81 | 0.002 | 0.007 | | |
| b ³ G | 4s3d ³ | 2.04 | <0.001 | 0.002 | | |
| Σ triplets ≥ 1.10 eV | | | 0.143 | 0.304 | 12 (4) ^c | 32 (11) ^c |

^aEnergies are averaged over J levels taken from ref 36. ^bMaxwell-Boltzmann distribution. Uncertainties due to the ± 100 K spread in filament temperatures are in parentheses. ^cEstimated value from VCH₂⁺ channel from ref 16.

the a⁵D ground state. Bond strengths of the product molecules VCH₃⁺, VCH₂⁺, and VCH⁺ were reported. Experimental results led to a proposed reaction mechanism in which the first step involves oxidative addition of the C-H bond at the metal center to form H-V⁺-CH₃. At low energies, H₂ is eliminated via a four-center transition state to form VCH₂⁺.¹⁶ At higher energies, cleavage of the V-H or V-C bond of the intermediate leads to production of VCH₃⁺ or VH⁺, respectively. VCH⁺ is formed primarily by loss of H₂ from the VCH₃⁺ product but also by loss of H from VCH₂⁺.

The major difference between CH₄ and NH₃ is the lone pair of electrons present on ammonia. We examine the effect that this lone pair has upon the cross-section magnitudes, ionic thermochemistry, and reaction mechanism by comparing this system to the methane system. The information gained may thus provide insight into the interaction of transition metals with such electrons and thereby improve the coordination chemist's view of metal-ligand bonding.

Experimental Section

General. A complete description of the apparatus and experimental procedures is given elsewhere.¹⁸ Briefly, the apparatus comprises three differentially pumped vacuum chambers. In the first chamber, ions are produced as described below. The resulting ions are extracted, accelerated, and focused into a magnetic sector momentum analyzer for mass analysis. In the second vacuum chamber, the mass-selected ions are decelerated to a desired kinetic energy and focused into an octopole ion guide. Radio frequency electric fields in the guide create a radial potential well which traps ions over the mass range studied. The velocity of the ions parallel to the axis of the guide is unchanged. The octopole passes through a static gas cell into which ammonia can be introduced. Pressures are maintained at a sufficiently low level (less than 0.2 mTorr) that multiple ion-molecule collisions are improbable. Product and unreacted beam ions are contained in the guide until they drift out of the gas cell. The ions are then extracted and focused into the third vacuum chamber which contains a quadrupole mass filter for product mass analysis. Ions are detected with a secondary electron scintillation ion detector and pulse-counting electronics. Raw ion intensities are converted to absolute cross sections as described previously.¹⁸ The accuracy of our absolute cross sections is estimated to be $\pm 20\%$. Uncertainties at low cross-section values are generally about $\pm 10^{-19}$ cm², primarily because of random counting noise (typically ≤ 10 counts/s).

Translational energies in the laboratory frame of reference are related to energies in the center of mass (CM) frame by $E_{\text{CM}} = E_{\text{lab}}m/(M+m)$, where M and m are the masses of the incident ion and neutral reactant, respectively. For these experiments, ⁵¹V (99.76% natural abundance) was used. The absolute energy scale and the ion kinetic energy distribution are determined by using the octopole beam guide as a retarding potential analyzer. Uncertainties in the absolute energy scale are ± 0.05 eV lab, and the fwhm of the energy distribution is 0.6 eV lab. Below ~ 0.6 eV

(3) Buckner, S. W.; Gord, J. R.; Freiser, B. S. *J. Am. Chem. Soc.* **1988**, *110*, 6606-6612.

(4) Radecki, B. D.; Allison, J. A. *J. Am. Chem. Soc.* **1984**, *106*, 946-952.

(5) Bryan, E. G.; Johnson, B. F. G.; Lewis, J. J. *Chem. Soc., Dalton Trans.* **1977**, 1328-1330.

(6) Armor, J. N. *Inorg. Chem.* **1978**, *17*, 203.

(7) Yamamoto, Y.; Yatagai, H.; Murayami, K. *J. Chem. Soc., Chem. Commun.* **1980**, 835-836.

(8) Hedden, D.; Roundhill, D. M.; Fultz, W. C.; Rheingold, A. L. *J. Am. Chem. Soc.* **1984**, *106*, 5014-5016.

(9) Hillhouse, G. L.; Bercaw, J. E. *J. Am. Chem. Soc.* **1984**, *106*, 5472-5478.

(10) Casalnuovo, A. L.; Calabrese, J. C.; Milstein, D. *Inorg. Chem.* **1987**, *26*, 971-973.

(11) Glueck, D. S.; Hollander, F. J.; Bergman, R. G. *J. Am. Chem. Soc.* **1989**, *111*, 2719-2722.

(12) Aristov, N.; Armentrout, P. B. *J. Am. Chem. Soc.* **1984**, *106*, 4065-4066.

(13) Aristov, N.; Armentrout, P. B. *J. Phys. Chem.* **1986**, *90*, 5135-5140.

(14) We use $\Delta_f H^\circ_{298}(\text{O}) = 59.55$ kcal/mol and $\Delta_f H^\circ_{298}(\text{H}_2\text{O}) = -57.80$ kcal/mol.¹⁵

(15) Chase, M. W.; Davies, C. A.; Downey, J. R.; Frurip, D. J.; McDonald, R. A.; Syverud, A. N. *J. Phys. Chem. Ref. Data* **1985**, *14*, suppl. 1 (JANAF Tables).

(16) Aristov, N.; Armentrout, P. B. *J. Phys. Chem.* **1987**, *91*, 6178-6188.

(17) Bent, H. A. *J. Chem. Educ.* **1966**, *43*, 170-186.

(18) Ervin, K. M.; Armentrout, P. B. *J. Chem. Phys.* **1985**, *83*, 166-189.

lab (0.15 eV CM), the energies are corrected for truncation of the ion beam energy distribution as described previously.¹⁸ The data obtained in this experiment are broadened by the ion energy spread and thermal motion of the neutral gas. The second effect, referred to as Doppler broadening, has a width (in eV) in the CM frame of $0.47E^{1/2}$ for the reaction of V^+ with NH_3 .¹⁹ When model cross sections are compared to experimental data, the calculated cross sections are convoluted with both sources of experimental energy broadening as described previously.¹⁸

Ion Sources. Vanadium ions are produced in two sources in these experiments. The primary source is a surface ionization (SI) source. Here, gaseous $VOCl_3$ (Alfa 99.995%) is directed at a resistively heated rhenium filament where decomposition of $VOCl_3$ and ionization of the resultant vanadium atoms takes place. The temperature of the filament is calibrated by optical pyrometry measurements and has an absolute uncertainty of ± 100 K. It is generally assumed that a Maxwell-Boltzmann distribution accurately describes the populations of the electronic states of the ions. The validity of this assumption has been discussed previously.²⁰ Table II gives these populations for V^+ at the filament temperatures used in these experiments.

The second source of ions used in these studies is an electron impact (EI) source. The electrons ionize and dissociate $VOCl_3$ vapor, leaving V^+ and other ions. The state populations are not characterized by a Maxwellian distribution since ionization is dominated by vertical processes. Since the appearance potential of V^+ from $VOCl_3$ is 26.8 ± 0.4 eV,²¹ it is possible to form significant percentages of excited-state ions at the electron energies of 30, 50, and 70 eV used in these experiments. This has been verified in previous experiments.^{16,22} The populations measured are included in Table II.

An electron impact/drift cell (DC) source²⁰ was also used in an attempt to electronically cool V^+ by collisions with methane. Although conditions in this source were such that the ions underwent over 1000 collisions with methane, noticeable contributions to the cross section from ions in excited electronic states were still observed.

The neutral gas used in this experiment was anhydrous ammonia (Matheson 99.99%). Before usage, three or more freeze-pump-thaw cycles with liquid nitrogen were done to remove volatile impurities.

Thermochemical Analyses. Theory²³ and experiment^{16,20,22-26} indicate that cross sections can be parametrized in the threshold region by eq 2, where σ_0 is a scaling factor, E is the relative

$$\sigma_T(E) = \sigma_0(E - E_T)^n / E^m \quad (2)$$

translational energy of the reactants, E_T is the reaction endothermicity, and n and m are adjustable parameters. As in previous studies,^{16,20,22} we have utilized eq 2 with $m = 1$. This form is expected to be the most appropriate for translationally driven reactions²⁷ and has been found to work exceptionally well in a number of previous studies of ion-molecule reactions.^{16,20,22-26} The other parameters (σ_0 , n , and E_T) are optimized by using a non-

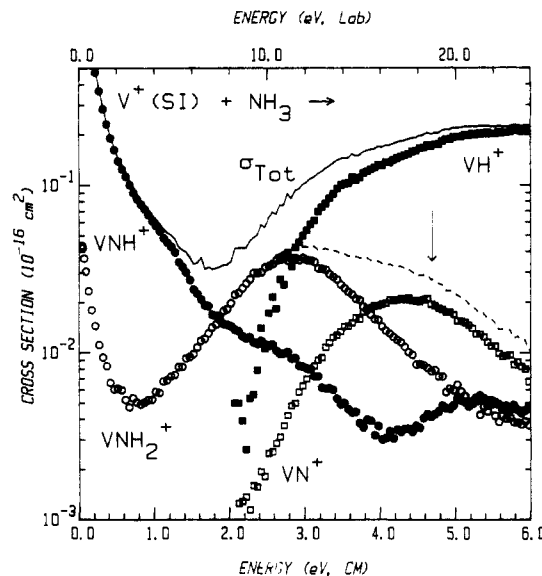


Figure 1. Variation of product cross sections for reaction of ammonia with V^+ produced by SI as a function of translational energy in the center-of-mass frame (lower scale) and laboratory frame (upper scale). The solid line is the sum of the cross sections for all products. The dashed line is the sum of $\sigma(VN^+)$ and $\sigma(VNH_2^+)$. The arrow at 4.69 eV shows the bond energy $D^0(H_2N-H)$.

linear least-squares analysis to give the best fit to the data. The cited threshold is the average of the analyses for all data sets. Conservative error limits for E_T are calculated from the range in these threshold values for different data sets and the error in the absolute energy scale (0.02 eV CM). These thresholds depend strongly upon the electronic state of the reactant ion and are converted to the threshold for the ground state, E_0 , by $E_0 = E_T + E_{el}$, where E_{el} is the average electronic energy of the reacting states. Analysis can also be accomplished by explicitly including the various states in eq 2. Such analyses yield E_0 values which are consistent within 0.03 eV with the values derived by correcting E_T with E_{el} .

For some data channels it is necessary to use a modified form of eq 2 which accounts for cross sections which decline due to dissociation of the product ion at higher energies. We have previously outlined such a model which makes a simple statistical assumption within the constraints of angular momentum conservation.²⁸ This empirical model defines P_D , the probability of dissociation of the product ion, as a function of E_D , the energy at which dissociation begins, and p , which is related to the number of internal modes in the transition state. Thus for $E < E_D$, P_D is zero, and for $E > E_D$, P_D asymptotically approaches 1. In this study, E_D is optimized to best fit the data. The parameter p (which is limited to integer values) is treated as a variable but the optimum value in this study is always 3.

Reaction threshold energies are converted to thermochemical values of interest by assuming that E_0 represents the enthalpy difference between reactants and products. This assumes that there are no activation barriers in excess of the endothermicity. This assumption is generally true for ion-molecule reactions, has been explicitly tested a number of times,²⁶ and appears to be a reasonable one in the present system as well. Furthermore, we implicitly assume that the neutral reactants and the products formed at the threshold of an endothermic reaction are characterized by a temperature of 298 K in all degrees of freedom. Thus, we make no correction for the energy available in internal modes of the neutral reactant.

Results

Four products, formed in reactions 3-6, are seen in the reaction of V^+ with NH_3 . Figure 1 shows the cross sections for these

(19) Chantry, P. J. *J. Chem. Phys.* **1971**, *55*, 2746-2759.

(20) Sunderlin, L. S.; Armentrout, P. B. *J. Phys. Chem.* **1988**, *92*, 1209-1219.

(21) Flesch, G. D.; Svec, H. *J. Inorg. Chem.* **1975**, *14*, 1817-1822.

(22) Elkind, J. L.; Armentrout, P. B. *J. Phys. Chem.* **1985**, *89*, 5626-5636.

(23) Aristov, N.; Armentrout, P. B. *J. Phys. Chem.* **1986**, *108*, 1806-1819.

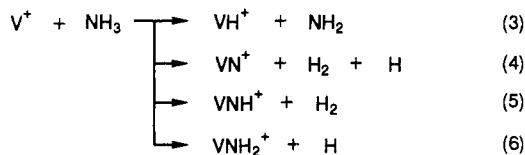
(24) Mandich, M. L.; Halle, L. F.; Beauchamp, J. L. *J. Am. Chem. Soc.* **1984**, *106*, 4403-4411. Armentrout, P. B.; Beauchamp, J. L. *J. Chem. Phys.* **1981**, *74*, 2819-2826. Halle, L. F.; Armentrout, P. B.; Beauchamp, J. L. *Organometallics* **1982**, *1*, 963-968. Armentrout, P. B.; Beauchamp, J. L. *J. Am. Chem. Soc.* **1981**, *103*, 784-791.

(25) Elkind, J. L.; Armentrout, P. B. *J. Phys. Chem.* **1986**, *90*, 5736-5745, 6576-6586; **1987**, *91*, 2037-2045; *J. Chem. Phys.* **1986**, *84*, 4862-4871; **1987**, *86*, 1868-1877.

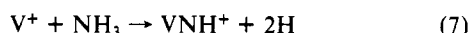
(26) Boo, B. H.; Armentrout, P. B. *J. Am. Chem. Soc.* **1987**, *109*, 3549-3559. Ervin, K. M.; Armentrout, P. B. *J. Chem. Phys.* **1986**, *84*, 6738-6749. Ervin, K. M.; Armentrout, P. B. *J. Chem. Phys.* **1987**, *86*, 2659-2673. Elkind, J. L.; Armentrout, P. B. *J. Phys. Chem.* **1984**, *88*, 5454-5456. Armentrout, P. B. In *Structure/Reactivity and Thermochemistry of Ions*; Ausloos, P.; Lias, S. G., Eds.; D. Reidel: Dordrecht, 1987; pp 97-164.

(27) Chesnavich, W. J.; Bowers, M. T. *J. Phys. Chem.* **1979**, *83*, 900-905.

(28) Weber, M. E.; Elkind, J. L.; Armentrout, P. B. *J. Chem. Phys.* **1986**, *84*, 1521-1529.

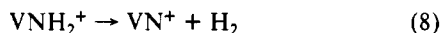


products when V⁺ is produced at a surface ionization (SI) filament temperature of 1950 K. (Comparable results are obtained for reaction with ND₃.) Below ~1.6 eV, reaction 5 dominates the reactivity. The fact that this cross section increases with decreasing energy to as low an energy as we can measure indicates that this reaction is exothermic, in agreement with BGF.³ To be exothermic, formation of VNH⁺ must be accompanied by production of the stable H₂ molecule. This is confirmed by noting that the VNH⁺ cross section also exhibits an endothermic feature with an apparent threshold of about 4.0 eV. This must be due to reaction 7, which is 4.5 eV = D^o(H₂) more endothermic than reaction 5.



The only other process observed at low energies is reaction 6, which actually dominates the reactivity over a brief energy range. The primary feature in this cross section is apparently endothermic with a threshold of ≈0.8 eV, but there is also a small exothermic component to this cross section. The endothermic feature peaks at about 2.8 eV. This is well below the energy needed to dissociate to V⁺ + NH₂ (4.69 eV, Table I), which is marked in Figure 1. The early peak could be due to dissociation to VN⁺ + H₂ which has a threshold at about this energy; however, as shown by the sum of σ(VNH₂⁺) and σ(VN⁺) (Figure 1) the magnitude of the VN⁺ cross section is too small to account completely for the decline in VNH₂⁺. The only remaining explanation is that the VH⁺ channel, reaction 3, is influencing the VNH₂⁺ cross section. This is consistent with the smooth appearance of the total cross section and is an indication that reactions 3 and 6 compete directly. At the highest energies, reaction 3 dominates the reactivity.

Reaction 4 is always a minor channel. One reason is that the VN⁺ product must be formed via decomposition of other products, reactions 8 and 9. Comparison of the magnitudes of σ(VNH₂⁺)



and σ(VNH⁺) to σ(VN⁺), Figure 1, suggest that σ(VNH⁺) is too small to account for the magnitude of σ(VN⁺). Further, we find that the sum of the VN⁺ and VNH₂⁺ cross sections (shown in Figure 1) falls off smoothly, consistent with VNH₂⁺ being the major contributor to VN⁺ formation via reaction 8. The change in slope in the summed cross section curve at 4.7 eV is due to dissociation of VNH₂⁺ to V⁺ + NH₂, which can begin at D^o(NH₂-H) = 4.69 eV. This dissociation channel is also reflected in the VN⁺ cross section, an observation which is further evidence for the parentage of VN⁺. Similar behavior can also be seen in the higher energy feature of VNH⁺. This is evidence that reaction 7 proceeds via decomposition of VNH₂⁺ to form VNH⁺ + H (the only plausible pathway).

As mentioned above, the electronic state of V⁺ can greatly affect the reaction cross section. In order to discuss these effects quantitatively, we examine SI and electron impact (EI) data for each individual product channel and derive state-specific cross sections when possible. Reaction thresholds are determined for each product channel and then used in the Discussion section to derive bond strengths for the product molecules.

VH⁺. The most efficient process above ~2.5 eV in the V⁺ + NH₃ reaction is the production of VH⁺. The SI cross sections for this product are independent of the filament temperature at which V⁺ is produced. Analysis of these SI data sets, Table III, give an average threshold of E_T = 2.52 ± 0.09 eV. When corrected for E_{e1} = 0.09 ± 0.02 eV, we find E₀ = 2.61 ± 0.09 eV. Given the value of D^o(NH₂-H) listed in Table I, this yields a bond energy for V⁺-H of 2.08 ± 0.09 eV, which is in excellent agreement with our previously reported VH⁺ bond energy of 2.09

TABLE III: Summary of Parameters of Eq 2 Used To Fit Threshold

| product ion | source ^a | E _T , eV | σ ₀ | n |
|-------------------------------|-------------------------|---------------------|----------------|-----------|
| VH ⁺ | SI 1950 K | 2.57 (0.04) | 0.36 (0.02) | 1.0 (0.1) |
| | SI 2200 K | 2.46 (0.03) | 0.44 (0.02) | 1.0 (0.1) |
| | EI 30 eV | 1.63 (0.08) | 3.35 (0.25) | 1.1 (0.1) |
| VN ⁺ | ⁵ X(SI) | 2.91 (0.06) | 0.066 (0.006) | 1.0 (0.1) |
| | EI 30 eV | 1.52 (0.12) | 0.46 (0.05) | 1.4 (0.4) |
| VNH ⁺ | ⁵ X(SI) | 4.33 (0.16) | 0.026 (0.003) | ≅1.0 |
| VNH ₂ ⁺ | ⁵ X(SI) | 1.47 (0.06) | 0.074 (0.005) | 1.6 (0.2) |
| | a ³ F(30 eV) | 0.38 (0.06) | 0.68 (0.01) | 1.8 (0.1) |

^aThis refers to the V⁺ source used to obtain the raw data analyzed. In cases where the ⁵X or a³F state is referred to, the text provides a complete description of the derivation of the cross section analyzed.

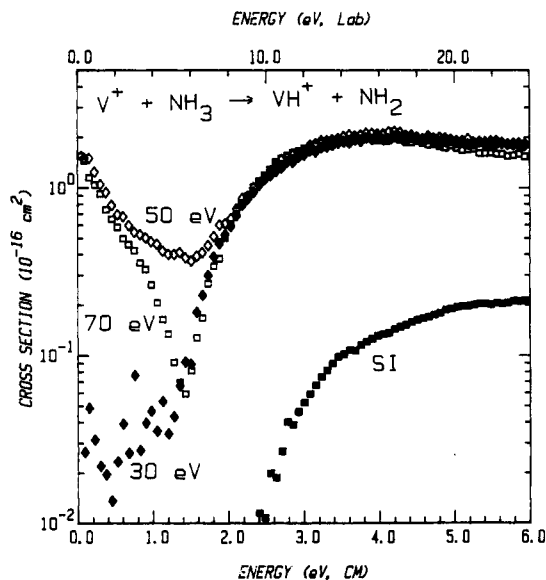


Figure 2. Kinetic energy dependence of σ(VH⁺) formed by reaction of ammonia with V⁺ produced by SI at 1950 K (■), by EI at 30 eV (◆), by EI at 50 eV (◇), and by EI at 70 eV (□) as a function of translational energy in the laboratory frame (upper axis) and the center-of-mass frame (lower axis).

± 0.06 eV.²² This agreement implies that this threshold is not subject to obvious systematic errors, such as misidentification of the reactive state(s) or activation barriers in excess of the endothermicity.

Figure 2 compares the VH⁺ cross section obtained from V⁺ formed in the SI source to those obtained for V⁺ formed with the EI source at electron energies of 30, 50, and 70 eV. The endothermicities, shapes, and magnitudes of the cross sections are clearly very dependent upon the source of V⁺. The 30-eV cross section is about an order of magnitude greater than the SI cross sections and is nonzero at the lowest energies we can measure. Analysis of the main endothermic feature of this cross section using eq 2 and the fitting parameters given in Table III yields a threshold of E_T = 1.63 ± 0.08 eV. Thus, E_{e1} = E₀ - E_T(30 eV) = 0.98 ± 0.12 eV, a value which roughly correlates to the excitation energy for the a³F state of 1.10 eV (Table II). Thus, we conclude that σ(VH⁺) from the 30-eV beam is dominated by V⁺(a³F). The nonzero contribution to the 30-eV cross section at energies below 1.63 eV indicates that states higher in energy than the a³F are also populated. AA have previously estimated the a³F population of the 30-eV beam to be 9 ± 3%. This estimate suggests that the cross section for VH⁺(a³F) is about a factor of 10 greater than the endothermic feature of the 30-eV cross section shown in Figure 2.

Increasing the electron energy from 30 to 50 eV significantly increases the low-energy cross section for VH⁺ formation. This is clearly an exothermic process which indicates that ions with electronic energies at least 2.5 eV above the ground state are contributing to the 50-eV VH⁺ cross section. At higher kinetic energies, the cross section has an apparent onset and magnitude

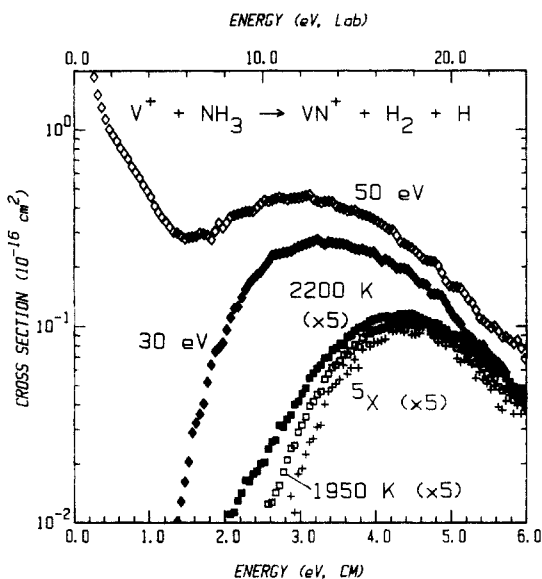


Figure 3. Kinetic energy dependence of $\sigma(\text{VN}^+)$ formed by reaction of ammonia with V^+ produced by SI at 1950 K (\square), SI at 2200 K (\blacksquare), EI at 30 eV (\blacklozenge), and EI at 50 eV (\diamond) as a function of translational energy in the laboratory frame (upper axis) and the center-of-mass frame (lower axis). The ^5X cross section (+) extrapolated from the SI data is also shown.

which matches the 30-eV data. Thus, this endothermic portion of the cross section is dominated by $\text{V}^+(\text{a}^3\text{F})$.

Upon increasing the electron energy from 50 to 70 eV, we observe that the magnitude of the exothermic portion of the cross section decreases. The endothermic portion has the same magnitude and apparent onset as the 30-eV data and thus corresponds to a^3F -state contribution. The decrease in the exothermic pathway indicates that the states contributing to that process have been depopulated.

At high kinetic energies, $\sigma(\text{VH}^+)$ could decline due to the decomposition to $\text{V}^+ + \text{H}$ which can begin at 4.69 eV (Table I). Since $\sigma(\text{VH}^+)$ does not decline at higher kinetic energies, the excess energy must be contained in either kinetic energy or internal modes of the NH_2 product. This is typical behavior for metal hydride ion products formed in reactions with alkanes.^{16,20,23}

VN^+ . The most endothermic process in the reaction of V^+ with ammonia is the formation of vanadium nitride ions, reaction 4. Figure 3 shows the 1950 and 2200 K SI cross sections for this reaction. At an energy near the threshold, 2.4 eV, the cross section is enhanced by a factor of ~ 2.3 when the SI filament temperature is increased from 1950 to 2200 K. The only plausible explanation for this enhancement is the increase in the population of the low-lying triplet states. Indeed, Table II shows that the populations of the a^3F and higher lying states increase by a factor of 2.1 as the filament temperature increases from 1950 to 2200 K. At higher kinetic energies, the magnitude of the cross section changes little with filament temperature, indicating that this reactivity is dominated by the a^5D - and a^5F -state ions.

Figure 3 also shows $\sigma(\text{VN}^+)$ formed from V^+ beams produced by EI with electron energies of 30 and 50 eV. The EI data have a greater magnitude than the SI data and show thresholds which have been shifted to lower energies. Specifically, the 30-eV cross section yields a threshold of 1.52 ± 0.12 eV when fit with the parameters given in Table III, and peaks at about 3.4 eV. This ~ 1 -eV shift in cross section peak position between the SI and 30-eV EI data correlates roughly to $E_{\text{el}}(\text{a}^3\text{F})$. Thus, the a^3F population of the 30-eV beam is apparently responsible for the peak position of the VN^+ cross section.

Upon increasing the EI electron energy from 30 to 50 eV, the magnitude of $\sigma(\text{VN}^+)$ is increased, and an exothermic as well as endothermic pathway to VN^+ formation is observed. The increase in magnitude again indicates that excited states make up an even greater portion of the 50-eV beam than the 30-eV beam. The exothermic pathway indicates that highly excited V^+ ions con-

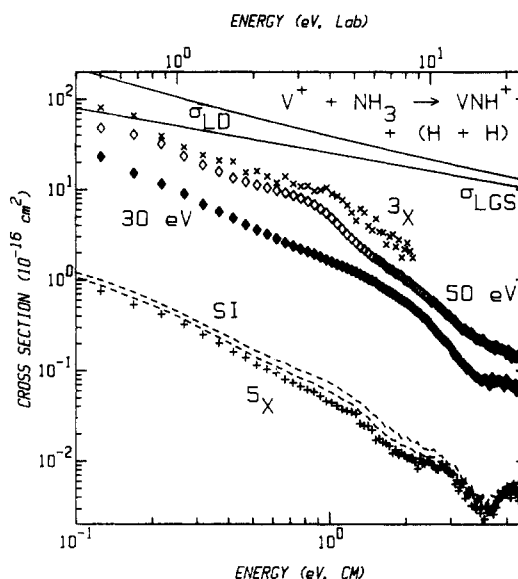


Figure 4. Kinetic energy dependence of $\sigma(\text{VNH}^+)$ formed by reaction of ammonia with V^+ produced by SI at 1950 K and 2200 K (dashed lines), EI at 30 eV (\blacklozenge), and EI at 50 eV (\diamond) as a function of translational energy in the laboratory frame (upper axis) and the center-of-mass frame (lower axis). The ^5X (+) and ^3X (x) cross sections extrapolated from the SI data, see text, are also shown. Full lines show the theoretical collision cross sections, σ_{LGS} and σ_{LD} .

tribute to VN^+ formation. Based on the 1.52-eV threshold for the 30-eV EI data, these ions must have at least 2.6 eV [$= 1.5 + E_{\text{el}}(\text{a}^3\text{F})$] internal excitation. The 70-eV EI data also show an exothermic as well as an endothermic process. The magnitudes of both features are similar to the 50-eV data.

Analysis of the VN^+ Cross Sections. Cross sections for production of VN^+ by the a^5D and a^5F states are derived by taking the 1950 and 2200 K SI data along with the populations of the excited triplet states given in Table II and extrapolating to a contribution of 0.0% of these states. This leaves a cross section (shown in Figure 3), due to reaction of only a^5D and a^5F ions, which we will refer to as the ^5X cross section since the relative reactivities of these two states cannot be unequivocally determined. This ^5X cross section can then be analyzed with eq 2 and the parameters in Table III and $E_{\text{D}} = 4.6$ eV. After correcting for $E_{\text{el}}(^5\text{X}) = 0.07 \pm 0.02$ eV, we obtain $E_0 = 2.98 \pm 0.06$ eV. By using the same values of n and m as for $\sigma(^3\text{X})$ and adjusting the threshold by $E_{\text{el}}(\text{a}^3\text{F})$, we can derive a model for the a^3F state. When added to the quintet-state model after appropriate scaling, Table II, both SI data sets are accurately reproduced.

As noted above, analysis of the 30-eV EI data yielded $E_{\text{T}} = 1.52$ eV. This suggests that the average value of E_{el} is 1.46 ± 0.13 eV, demonstrating that states above the a^3F are contributing to this cross section. The a^3P state is probably significant since $E_{\text{el}}(\text{a}^3\text{P}) = 1.45$ eV, Table II. By combining appropriate amounts of model cross sections for the a^3F and a^3P states (again using the same values of n and m as for $\sigma(^3\text{X})$ and adjusting the threshold by E_{el}), the 30-eV data can also be reproduced.

VNH^+ . The dominant process at low energies in the reaction of V^+ with ammonia is reaction 5. Figure 4 shows SI cross sections at two filament temperatures for this reaction. Both SI data sets show exothermic reactivity which clearly increases with the filament temperature. However, the ratio of cross sections for the 1950 and 2200 K data is only 1.0 to 1.3. This is slightly more than can be accounted for by the a^5F state but much less than expected for the a^3F and higher states. Thus, the major portion of the magnitude of the exothermic process is dominated by reaction of the a^5D - and a^5F -state ions.

Also shown in Figure 4 are the VNH^+ cross sections produced from V^+ formed in the 30- and 50-eV EI sources. As with the VH^+ and VN^+ channels, the 30-eV cross section has a much greater magnitude than the SI data. At 50 (and also 70 eV), the magnitude of the cross sections is enhanced further. The endo-

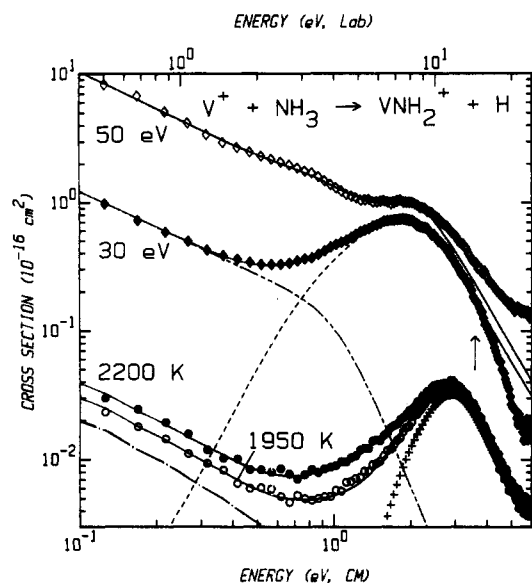


Figure 5. Kinetic energy dependence of $\sigma(\text{VNH}_2^+)$ formed by reaction of ammonia with V^+ produced by SI at 1950 K (O), SI at 2200 K (●), EI at 30 eV (◆), and EI at 50 eV (◇) as a function of translational energy in the laboratory frame (upper axis) and the center-of-mass frame (lower axis). The dashed line and double-dash line show the contributions of the $a^3\text{F}$ and higher lying states, respectively, to the 30-eV cross section. The arrow at 3.59 eV shows the bond energy $D^0(\text{H}_2\text{N-H}) - E_{\text{el}}(a^3\text{F})$. Contributions to the SI data from the ^5X (+) and $\sigma(\text{VO}^+)$ (dash-dot line) are also shown.

thermic feature of $\sigma(\text{VNH}^+)$ observed in the SI data is less prominent in the EI data. This is due to the large magnitude increase in the exothermic EI cross section which masks the smaller decomposition pathway, reaction 7.

Analysis of the VNH^+ Cross Sections. In order to derive a cross section representative of the $a^5\text{D}$ and $a^3\text{F}$ states, we again extrapolate the SI data to a contribution of 0.0% of the excited triplet states. This ^5X cross section is shown in Figure 4. For this large reaction channel, the data is sufficiently good that we can also extrapolate to 100%, thus generating a cross section for the triplet states, ^3X , also shown in Figure 4.²⁹ The validity of this extrapolation is supported by comparison of the 30-eV data to this latter extrapolated cross section. This comparison shows that the shapes are nearly identical, consistent with expectations based on the reaction channels discussed above. Also, the 30-eV data has a magnitude which is $24 \pm 5\%$ of the extrapolated ^3X cross section. Thus, the population of excited triplet states in the 30 eV beam is $24 \pm 5\%$, consistent with the estimate given by AA, $21 \pm 5\%$ (Table II).

The ^5X cross section shows that reaction 5 is exothermic with a small endothermic feature at high energies. This establishes that the reaction of the $\text{V}^+(a^5\text{F})$ state is exothermic such that $D^0(\text{V}^+-\text{NH}) \leq 3.81$ eV ($=4.17-0.36$). A more precise value of this bond energy can be obtained by analyzing the cross section for reaction 7, the endothermic feature observed in the SI data for VNH^+ . We arrive at the threshold for this feature by the following method. The exothermic portion of the ^5X cross section (and also the raw SI data) was fit in the energy region below the endothermic feature (between ~ 2.8 and 3.9 eV) with a power law and this was subtracted from the cross section, leaving only the endothermic feature. This feature was then analyzed with eq 2 by using the parameters given in Table III. The threshold for this feature, after correction for E_{el} , yields $E_0 = 4.40 \pm 0.16$ eV. Since the bond energy of H_2 is 4.52 eV, this value is consistent with the exothermicity of reaction 5 for $\text{V}^+(a^5\text{F})$ and establishes that reaction of $a^5\text{D}$ ground-state ions is also exothermic.

VNH_2^+ . Figure 5 shows VNH_2^+ cross sections from V^+ produced by the SI source with filament temperatures of 1950 and

2200 K. Clearly, the exothermic portions of these cross sections depend on temperature while the endothermic feature, which peaks at ~ 2.8 eV, does not. At 1 eV, the 1950 and 2200 K cross sections have magnitudes of about 0.005 and 0.009 \AA^2 , respectively, a ratio of 1.0:1.8. Table II shows that the fraction of the $a^5\text{D}$ state decreases as the temperature is increased, while the $a^3\text{F}$ increases by a factor of only 1.2. Thus, the differences between the 1950 and 2200 K data must be due largely to the $\sim 10^{-3}$ fraction of the beam in excited triplet states. Table II shows that the $a^3\text{F}$ population increases by a factor of 2.0, while higher lying states increase by a factor of 2.7. Thus, the dominant contribution to the cross section in this energy region must come from the $a^3\text{F}$. The higher energy states may also contribute to the exothermic cross section but cannot quantitatively account for the temperature dependence.

Also shown in Figure 5 are the VNH_2^+ cross sections obtained by using the EI source with electron energies of 30 and 50 eV. As in the other channels, these cross sections show an increase in magnitude when compared with the SI data. The 30-eV cross section peaks at ~ 1.8 eV, about 1 eV lower than the peak in the SI data. This 1-eV shift in peak position correlates well to $E_{\text{el}}(a^3\text{F})$ and suggests that the endothermic portion of the 30-eV data is due to reaction of the $a^3\text{F}$ state. Therefore, the exothermic feature is presumed to be due to reaction of $a^3\text{P}$ or higher states.

Increasing the electron energy from 30 to 50 eV increases the low-energy exothermic feature of this cross section by about an order of magnitude. This helps confirm the identification of this feature as coming from $a^3\text{P}$ states or higher since AA made a similar state identification by observing similar effects in going from 30 to 50 eV EI conditions for the reaction $\text{V}^+ + \text{CH}_4 \rightarrow \text{VCH}_2^+ + \text{H}_2$ (a reaction which has similar energetics to reaction 6).¹⁶ A curious feature of the 50-eV data is that this change in electron energy also gives rise to enhanced VNH_2^+ production at high kinetic energies (>3 eV). The increase at high energies does not correspond to either the SI or 30-eV EI cross-section shape and must therefore be due to a higher energy state(s).

Increasing the electron energy from 50 to 70 eV has little effect on the magnitude of the low-energy feature of the cross section but does increase the very high energy feature to a cross section of 0.4 \AA^2 at 6 eV. This increase is consistent with highly excited states accounting for this feature. Since these states appear to react most efficiently at kinetic energies above ~ 3 eV, this suggests that these states either exhibit an activation barrier, or produce excited $\text{VNH}_2^+ + \text{H}$ products in an endothermic reaction.

Analysis of the VNH_2^+ Cross Sections. In order to obtain E_0 and elucidate a V^+-NH_2 bond strength, we need to understand how the different electronic states of V^+ contribute to reaction 6. Since the 30- and 50-eV data sets have different amounts of the endothermic $a^3\text{F}$ feature and the exothermic feature due to higher excited states, they can be used to derive model cross sections for these two features.³⁰ These are shown in Figure 5. We find that the exothermic portion declines as $E^{-0.94 \pm 0.05}$ until $E_D \approx 0.88$ eV, where it falls off as E^{-3} . The endothermic portion can be analyzed by using eq 2 with the parameters in Table III to give a value of $E_T = 0.38 \pm 0.06$ eV and $E_D = 1.9$ eV. Assuming that the $a^3\text{F}$ state is the only contributor to this derived endothermic cross section means that $E_0 = 1.48 \pm 0.06$ eV, a value which implies that states with $E_{\text{el}} > 1.48$ eV react exothermically. This includes all higher lying states with the possible exception of $\text{V}^+(a^3\text{P})$ (Table II). If the $a^3\text{P}$ reaction is endothermic, our analysis would lead to a higher value for E_0 depending on the relative contributions of the $a^3\text{F}$ and $a^3\text{P}$ states to the endothermic feature. We have verified that these changes in E_0 are small as long as the $a^3\text{F}$ state is the dominant contributor to the endothermic feature (which seems likely based on results for other product channels). Analysis of the SI cross sections (below) also helps confirm this assumption.

(29) Technically, there may be contributions from the $a^3\text{P}$ state in this cross section. It is likely that such contributions are small since the reactivity of the quintet states is much smaller than the triplet states.

(30) By scaling the 50- and 70-eV EI data to the 30-eV data at low energies and subtracting, a cross section proportional to the endothermic $a^3\text{F}$ feature can be derived. This can then be subtracted from the 30-, 50-, and 70-eV EI data to yield the exothermic cross section feature.

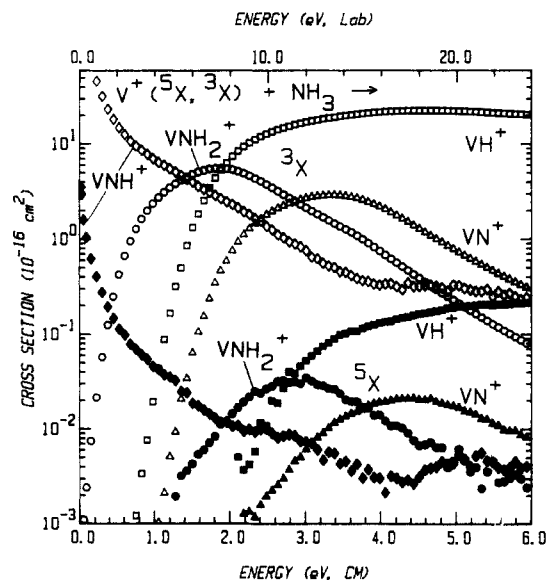


Figure 6. State-specific cross sections for the reaction of ammonia with V^+ as a function of translational energy in the laboratory (upper axis) and center-of-mass frame (lower axis). Solid and open symbols show results for $V^+(^5X)$ and for $V^+(a^3F, ^3X)$, respectively, derived as discussed in the text. In both cases, squares represent the VH^+ product, triangles represent the VN^+ product, diamonds represent the VNH^+ product, and circles represent the VNH_2^+ product.

For the SI data, the dominant contribution to the observed cross section comes from the low-lying a^3D and a^3F states. However, below ~ 1.1 eV [$=E_0 - E_{el}(a^3F)$], excited states with $E_{el} \geq 1.10$ eV must account for the observed SI cross sections. This contribution is removed by extrapolating to 0.0% of the sum of these states by using the populations in Table II. The remaining cross section is dominated by an endothermic feature beginning at about 1.5 eV,³¹ which must be due to reaction of $V^+(a^3D, a^3F)$. Analysis of this feature using eq 2 with the fitting parameters given in Table III gives a value of $E_T = 1.47 \pm 0.06$ eV and $E_D = 2.9$ eV. Note that the value of n used here is similar to that found above for the a^3F state and that the values of E_T and E_D differ by ~ 1.0 eV, consistent with the difference in the electronic states involved, $E_{el}(a^3F) - E_{el}(^5X) = 1.03$ eV. The good agreement in these results lends confidence to the state assignments made in deriving them. We conclude that the average of these two interpretations provides the best determination of E_0 for reaction 6, 1.51 ± 0.10 eV.

As a final check of the manipulations described above, Figure 5 shows that the SI and EI data can be accurately reproduced by combining appropriately scaled models (using the populations of Table II and the parameters given in Table III and an average value for E_0) for the quintet states, the a^3F state, and the exothermic higher states (and for the SI data, a small contribution from VO^+). As can be seen in Figure 5, the reproduction is excellent except at the highest energies for the 30- and 50-eV EI data. At these energies, the 30-eV cross section is smaller than its model, while the 50-eV data is larger than its model. The 50-eV enhancement at high energies has been discussed above and is attributed to a highly excited state(s) that reacts efficiently at energies above ~ 3 eV. The 30-eV deviation can be explained

(31) This extrapolated cross section also shows a small exothermic feature. Additional experiments demonstrate that this is almost certainly due to formation of VO^+ (having the same mass as VNH_2^+) from the reaction of V^+ with residual O_2 or H_2O . While the magnitude of this contribution is small ($< 4 \times 10^{-4}$ of the cross section for the reaction of $V^+ + O_2$), it does distort the low-energy VNH_2^+ cross section. We account for this by subtracting appropriately scaled $\sigma(VO^+)$ from the extrapolated cross section. Examination of several SI data sets taken at different times shows that the extent of VO^+ contamination varies; however, the endothermic feature which remains after subtraction of the VO^+ contribution has the same magnitude, shape, and threshold (within 0.05 eV) for all data sets. This analysis of the data is also verified by results for VND_2^+ produced from reaction of V^+ with ND_3 , where there is no VO^+ contamination. In the EI data, the exothermic VNH_2^+ cross sections are sufficiently large that contributions from VO^+ are negligible.

by the dissociation process $VNH_2^+ \rightarrow V^+ + NH_2$. For $V^+(a^3F)$, this process can begin at $D^0(NH_2-H) - E_{el}(a^3F) = 3.59$ eV, in good agreement with the onset of the deviation, Figure 5.

State-Specific Cross Sections. For each of the reactions discussed above, it was possible to derive a cross section for the a^3D and a^3F states and for excited states, usually the a^3F state. The former cross section, which we will term 5X , is shown in Figure 6. These cross sections are basically those of the SI data with small contributions from excited states removed. Thus, the absolute magnitudes and shapes of these cross sections are in little doubt. For the excited states, also shown in Figure 6, the absolute cross sections are less certain but are certainly accurate to within a factor of ~ 3 . These cross sections were derived as follows. The VH^+ cross section was derived by taking the model cross section for the 30-eV EI data and correcting the absolute magnitude by using AA's estimate for the population of the a^3F state (Table II). For the VN^+ and VNH_2^+ cross sections, the models used to reproduce the a^3F contributions to the SI cross sections were scaled by the populations in Table II to obtain absolute a^3F cross sections. A check on the internal consistency of this procedure is to use this absolute a^3F cross section to estimate the population of this state in the 30-eV EI data. We find that this comparison suggests a $\sim 13\%$ population for $\sigma(VNH_2^+)$ and $\sim 10\%$ for $\sigma(VN^+)$, in good agreement with AA's value of $9 \pm 3\%$. As a cautionary note, we find that if the 50-eV EI data is similarly used, the absolute cross section for VNH_2^+ derived is about 3 times larger than the one shown. This is probably an accurate measure of the absolute uncertainties in these derived cross sections. In the case of VNH_2^+ , the cross section shown includes a model which accounts for the observed decline in the cross section at high energies due to dissociation of $VNH_2^+ \rightarrow V^+ + NH_2$, beginning at 3.59 eV $= D^0(NH_2-H) - E_{el}(a^3F)$. Finally, for the VNH^+ cross section, we cannot extract a cross section due solely to reaction of $V^+(a^3F)$ since all states react exothermically to form VNH^+ . Therefore, we have used a sum of the triplet states, as discussed above, and extrapolated to procure $\sigma(VNH^+, ^3X)$. As shown in Figure 4, this manipulation leads to fairly large scatter, although the shape of the cross section is equivalent to that of the 30-eV EI data. Therefore, Figure 6 shows this latter data scaled to the appropriate absolute magnitude.

The most striking feature of Figure 6 is the large increase in the magnitude of $\sigma(^3X)$ when compared with $\sigma(^5X)$. On the basis of the VN^+ and VNH_2^+ cross sections, we estimate that $V^+(a^3F)$ is more reactive than $V^+(^5X)$ by factors of 110 and 170, respectively. The VNH^+ channel shows that the reactivity of $V^+(^3X)$ is greater than that of $V^+(^5X)$ by a factor of ~ 160 . This enhancement in reactivity is comparable to the effect observed by AA for the dehydrogenation reaction of methane by these states of V^+ .

Figure 6 also shows that the competitions between the reaction channels discussed above for the 1950 K SI data, which is primarily due to reaction of $V^+(^5X)$, are also apparent for $V^+(^3X)$. Specifically, it can be seen that the peak in $\sigma(VNH_2^+)$ occurs near the threshold for $\sigma(VH^+)$ for both states. The sizes of $\sigma(VN^+)$ and the high-energy component of $\sigma(VNH^+)$ relative to $\sigma(VNH_2^+)$ are similar for both states. In all cases, the thresholds and peaks of the cross sections are energy shifted by slightly more than 1 eV $\approx E_{el}(a^3F)$. This similarity in behavior indicates that the reaction mechanisms of both quintet and triplet states are the same.

Reaction Efficiency. Comparison of the 5X cross section with σ_{LGS} indicates that these states react with $\sim 1\%$ efficiency at our lowest energies (≈ 0.1 eV). By averaging our experimental cross sections over a Maxwell-Boltzmann distribution, we can determine a thermal rate constant¹⁸ which is 9.8×10^{-12} cm³/s, 1% of that of the total collision rate. This is somewhat lower than the 5% efficiency value given by BGF³ and suggests that they have excited-state V^+ contributing to their observed reaction rate. This is a reasonable possibility since BGF produced their vanadium ions by laser desorption/ionization.

The 3X cross section is comparable to σ_{LGS} at the lowest energies (this is most easily seen in Figure 4), which suggests that these

excited states react with near unit efficiency. However, ammonia has an appreciable dipole moment (1.47 D) such that the collision frequency should actually be higher than predicted by σ_{LGS} . A reasonable upper limit to the true collision cross section is easily calculated for the locked dipole model,³² σ_{LD} . We find that, below 1.0 eV, the ³X cross section behaves as $\sim 0.25(\sigma_{\text{LD}})$.

Discussion

Thermochemistry. Bond energies for V⁺-H (2.08 ± 0.09 eV), V⁺-N (4.65 ± 0.06 eV), V⁺-NH (4.30 ± 0.16 eV), and V⁺-NH₂ (3.18 ± 0.10 eV) are derived from the ammonia thermochemistry listed in Table II and E₀ values for reactions 3, 4, 7, and 6 (2.61 ± 0.09, 2.98 ± 0.06, 4.40 ± 0.16, and 1.51 ± 0.10 eV, respectively). The VH⁺ bond energy determined here agrees well with a previous value, 2.09 ± 0.06 eV.²² Our VN⁺ bond energy is considerably higher than the 3.78 eV value calculated by Kunze and Harrison; however, these authors note that their absolute bond energies are generally low by about 25%.³³ Correcting their result by this factor provides an estimated bond energy of ~ 4.7 eV, in good agreement with our experimental result. Our VNH⁺ value also agrees with the limits of 4.17 eV ≤ D°(V⁺-NH) ≤ 5.17 eV derived from BGF's work³ as described in the Introduction, as well as their stated result of 4.38 ± 0.30 eV.

We can also compare our value for D°(VN⁺) = 4.65 ± 0.06 eV to literature values of D°(VN) = 4.95 ± 0.09 eV³⁴ and 4.82 ± 0.22 eV.³⁵ Using these bond strengths and the ionization potential of vanadium, IP(V) = 6.740 ± 0.002 eV,³⁶ eq 10 can be used to calculate IP(VN) = 7.04 ± 0.11 or 6.91 ± 0.23 eV,

$$\text{IP(VN)} = D^\circ(\text{VN}) + \text{IP(V)} - D^\circ(\text{VN}^+) \quad (10)$$

in agreement with the rough experimental value of 8 ± 1 eV.³⁴ Since the IPs of V and VN are similar, ionization of VN probably involves the removal of an electron from a nonbonding metal orbital.

The bond energies D°(VN⁺-H) = 3.10 ± 0.17 eV and D°(VNH⁺-H) = 2.88 ± 0.19 eV can also be calculated from our data. Note that both values are significantly stronger than D°(V⁺-H) and much more similar to D°(N-H) = 3.46 eV. This is consistent with the V⁺-NH and V⁺-NH₂ structures rather than H-V⁺-N and H-V⁺-NH. Also the value of D°(VN⁺-H) can be combined with IP(VN) and IP(H) = 13.598 eV¹⁵ to calculate the proton affinity of VN, PA(VN). Depending on the value of IP(VN) used, the result is either 9.66 ± 0.20 eV = 223 ± 5 kcal/mol or 9.79 ± 0.29 eV = 226 ± 7 kcal/mol. Both values are in good agreement with BGF's direct measurement of 220 ± 6 kcal/mol.³ Actually, BGF determined that VNH⁺ did proton transfer to diethylamine but not to pyridine. Using updated values for the proton affinities of these molecules, 225.9 and 220.8 kcal/mol,^{37,38} respectively, it can be seen that our values for PA(VN) are in excellent agreement with the BGF experimental results.

Bond Energy-Bond Order Correlation. In a previous study,¹² we have pointed out that a qualitative feeling for the bonding character in simple transition-metal-ion-ligand species can be obtained by a comparison of their bond strengths with analogous bonds in carbon systems. We found that there was a reasonable correlation between V⁺-CH_n (n = 0-3) and CH_n-CH_n bond strengths. Figure 7 shows this correlation for the updated thermochemistry given in Table IV and the present results for V⁺-NH_n (n = 0-2) compared to both D°(CH_{n+1}-NH_n) and D°(NH_n-NH_n). The latter comparison is included to demonstrate that the

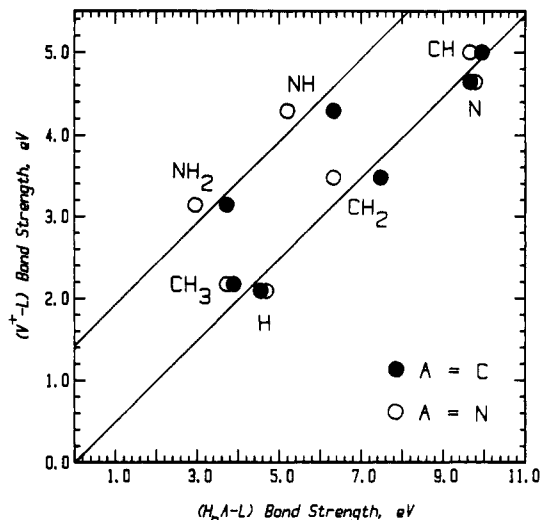


Figure 7. Bond dissociation energies from Table IV for V⁺-L vs H_nA-L, where L is the group indicated. Reference bond energies are indicated for A = C (closed circles) and for A = N (open circles). The lower line shows the result of a linear regression fit (slope = 0.50) of all data but L = NH and NH₂. The upper line is a best fit to the L = NH and NH₂ data while retaining the slope of 0.50.

TABLE IV: Heats of Formation and Bond Dissociation Energies (eV) at 298 K

| M ⁺ -L | Δ _f H°(ML ⁺) ^a | D°(M ⁺ -L) ^b | D°(CH _n -L) ^c | D°(NH _n -L) ^c |
|---------------------------------|--|---|-------------------------------------|-------------------------------------|
| V ⁺ -H | 12.32 (0.10) | 2.09 (0.06) ^d 2.08 (0.09) | 4.55 (0.02) | 4.69 (0.01) |
| V ⁺ -CH | 13.30 (0.10) | 5.00 (0.06) ^e | 9.95 (0.18) | |
| V ⁺ -CH ₂ | 12.68 (0.17) | 3.47 (0.14) ^e | 7.47 (0.06) | |
| V ⁺ -CH ₃ | 11.49 (0.13) | 2.17 (0.10) ^e | 3.89 (0.02) | |
| V ⁺ -N | 12.40 (0.10) | 4.65 (0.06) | 9.66 (0.20) | 9.78 (0.002) |
| V ⁺ -NH | 11.55 (0.18) | 4.30 (0.16) 4.38 (0.30) ^f | 6.32 (0.16) | 5.19 (0.11) |
| VN ⁺ -H | 11.55 (0.18) | 3.10 (0.17) | | |
| V ⁺ -NH ₂ | 10.93 (0.13) | 3.18 (0.10) | 3.72 (0.02) | 2.95 (0.01) |
| VNH ⁺ -H | 10.93 (0.13) | 2.88 (0.19) | | |

^a Ion heats of formation are calculated by using the thermal electron convention. Δ_fH°(V⁺) = 12.15 (0.08) eV, ref 15. ^b Values are from this study unless otherwise noted. ^c Bond energies for these species are calculated by using heats of formation from ref 15 and: Pedley, J. B.; Naylor, R. D.; Kirby, S. P. *Thermochemical Data of Organic Compounds*, 2nd ed.; Chapman and Hall: London, 1986. The only exception is that Δ_fH°(CH₂NH) = 32 ± 2 kcal/mol was taken from ref 38. ^d Reference 22. ^e Reference 16. ^f Reference 3.

trends shown are general and can be extended to various neutral molecules with similar bonding characteristics.

Figure 7 shows that the bond strength of V⁺-N agrees readily with the trend seen for the carbon ligands and falls in the region associated with covalent triple bonds. Since V⁺ has four valence electrons, a triple bond implies that VN⁺ should have a single unpaired electron on the metal and thus should have a doublet ground state. Indeed, Kunze and Harrison calculate that the ground state is ²Δ containing a V-N triple bond.³³

In contrast, the bond strengths of V⁺-NH₂ and V⁺-NH are markedly higher than their isoelectronic analogues, V⁺-CH₃ and V⁺-CH₂. Thus, the nitrogen lone pair electrons must be contributing to the bonding, which implies a significant overlap between the lone pair and the empty metal d orbitals. In effect, this appears to form an additional bond worth about 1.4 eV (based on the y intercept of the upper line in Figure 7). The end result is a V⁺-NH₂ bond energy comparable in strength to a V⁺-C double bond and a V⁺-NH bond energy nearly equal to the V⁺-N triple bond. (Using an identical analysis, BGF came to the different conclusion that VNH⁺ had only a double bond,³ in part because they plotted their lower limit of 4.0 eV on a plot similar to Figure 7.) This bonding picture implies that VNH⁺ and VNH₂⁺ have triplet and quartet ground states, respectively.

Reaction Mechanism. In this section, the information presented above is used to postulate a mechanism for the reaction of V⁺ with

(32) Su, T.; Bowers, M. T. *Gas Phase Ion Chemistry*; Bowers, M. T., Ed.; Academic: New York, 1979; pp 84-117.

(33) Kunze, K. L.; Harrison, J. F. *J. Phys. Chem.* **1989**, *93*, 2983-2997.

(34) Farber, M.; Srivastava, R. D. *J. Chem. Soc., Faraday Trans. 1* **1973**, *69*, 390-398.

(35) This value comes from the JANAF Tables, ref 15, where the data of ref 34 was reevaluated.

(36) Sugar, J.; Corliss, C. *J. Phys. Chem. Ref. Data* **1985**, *14*, Suppl. No. 2.

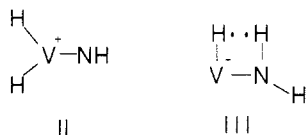
(37) Lias, S. G.; Liebman, J. F.; Levin, R. D. *J. Phys. Chem. Ref. Data* **1984**, *13*, 695-808.

(38) Lias, S. G.; Bartmess, J. E.; Liebman, J. F.; Holmes, J. L.; Levin, R. D.; Mallard, W. G. *J. Phys. Chem. Ref. Data* **1988**, *17*, Suppl. 1.

ammonia. This mechanism must not only explain the observed products but also the dependence of the reactions on electronic excitation. The mechanism we favor is directly analogous to that proposed to explain the interaction of V^+ with methane.¹⁶

A simple reaction mechanism for the interaction of V^+ with ammonia involves oxidative addition of the N-H bond at the metal center to form intermediate I, $H-V^+-NH_2$. Bond additivity arguments can be used to estimate that the reaction leading to this intermediate is ~ 0.6 eV exothermic. Intermediate I clearly explains the observed competition between the VH^+ and VNH_2^+ products. Formation of VNH_2^+ dominates at low energies because it is thermodynamically favored. Formation of VH^+ dominates at high energies since it is strongly favored by angular momentum constraints. This argument has been detailed previously¹⁶ and can be seen qualitatively by comparing the reduced masses of the reactants and products. For reaction 3, the reduced masses of the reactants, $\mu(V^+ + NH_3) = 12.8$ amu, and the products, $\mu(VH^+ + NH_2) = 12.2$ amu, are nearly equal and it is therefore easy to conserve orbital angular momentum. However, for reaction 6, the reduced mass of the products, $\mu(VNH_2^+ + H) = 1.0$ amu, is much smaller such that orbital angular momentum cannot be conserved for large reactant impact parameters. The result is that the latter channel is more highly restricted than the former channel. Reactions 4 and 7 can be explained by decomposition reactions involving the products formed via intermediate I, as mentioned above.

Intermediate I is also an obvious first step in the dehydrogenation reaction. We envision two possible mechanisms for the dehydrogenation step starting from I: via intermediate II or the four-center transition state III. There are three reasons that we



think II is an unlikely pathway for reaction 5. First, by using bond additivity arguments, we estimate that the production of II from $V^+(a^5D) + NH_3$ is endothermic by $\sim 0.2 \pm 0.2$ eV. Since formation of VNH^+ occurs exothermically with no activation barrier, this argument discounts intermediate II as a viable pathway (but not definitively). Second, BGF have observed that the analogue of reaction 5 also occurs for Sc^+ ,³ and we have verified that the behavior of the Sc^+ + ammonia system is very similar to that of V^+ .³⁹ Since Sc^+ has only two valence electrons, it cannot support the three covalent bonds of II. Even if a the Sc^+-H bonds are covalent and the H_2Sc^+-NH bond is dative, formation of the scandium analogue of II is estimated to require 0.6–2 eV in excess of the $Sc^+ + NH_3$ reactants. Third, using arguments similar to the first two, the $H_2V^+-CH_2$ intermediate analogous to II has been discounted as an intermediate for dehydrogenation of methane (and here the first argument is much more definitive).¹⁶ Since the state-specific behavior of the reactions of V^+ with methane and ammonia parallel one another, it seems reasonable that the mechanisms are also analogous.

If we use the same three criteria to evaluate intermediate III, we conclude it is a viable pathway for dehydrogenation. First, bond additivity estimates suggest that formation of III requires no energy in excess of the reactants (a reverse activation barrier of 0.12 ± 0.16 eV). While this may at first appear to be a small activation barrier for a four-center reaction, ordinarily symmetry forbidden, calculations have demonstrated that such an elimination can be facile if the transition-metal ligand bonds are covalent and have significant d character.⁴⁰ Both of these conditions are probably met by intermediate I. Second, the analogous four-center intermediate in the scandium system will have comparable energetics to III since only two metal electrons are ever involved

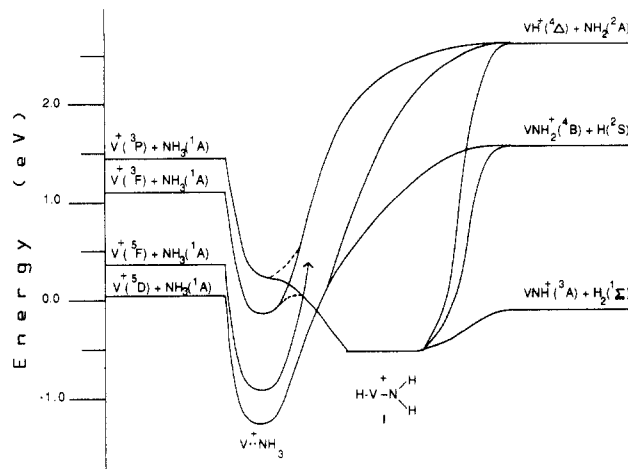


Figure 8. Semiquantitative potential energy diagram for the interaction of V^+ with ammonia. Dashed lines show avoided crossings between surfaces having the same spin.

in the bonding. Third, this mechanism directly parallels that for the methane system.

Another potential mechanism for reaction 5 is 1,1-dehydrogenation directly from the adduct, V^+-NH_3 . While this mechanism cannot be excluded unambiguously, we discount it for two reasons. First, we again appeal to the analogy between the methane and ammonia systems. Since no strongly bound adduct can be formed in the former system, the adduct seems less likely to be the critical intermediate. Second, close examination of the SI and 5X cross sections for VNH^+ , Figures 1 and 4, shows that these cross sections have downward breaks at energies of about 1.4 and 2.8 eV, corresponding to the onsets for VNH_2^+ and VH^+ production, respectively. This demonstrates that these three products all share a common intermediate. This intermediate could be I, as suggested above, or the adduct. However, the adduct does not provide an easy explanation for the electronic-state dependence in these reactions, while intermediate I does. This analysis is detailed in the next section.

Electronic-State Dependence. In order to understand the effects of electronic states upon product formation, molecular orbital ideas can be employed. These arguments have been used successfully before in the reactions of atomic metal ions with H_2 ²² and CH_4 ,¹⁶ elucidating reactivities and mechanisms. Oxidative addition of N-H to a metal center is achieved by donation of electrons in σ bonding orbitals into empty 4s and 3d σ orbitals of the metal and back-donation of the metal 3d π electrons into σ^* antibonding orbitals. This increases the electron density between the metal and molecular fragments and also lengthens the N-H bond. For V^+ , the states having 3d⁴ configurations, e.g., a^5D , a^3P , and higher triplet states, can interact with NH_3 in this way and therefore should have attractive potential energy surfaces. However, if the metal 4s orbital (and to a lesser extent the 3d σ) is occupied, the surfaces will be repulsive since the 4s orbital correlates to an antibonding orbital of the intermediate. Thus, states such as $a^5F(4s3d^3)$ and $a^3F(4s3d^3)$ are anticipated to be less reactive than those with empty 4s and 3d σ orbitals.

Further insight into the V^+ with ammonia system can be gained by examining the potential energy surfaces involved. In order to do this, the spin state of intermediate I must be established. If I truly contains covalent V-H and V-N bonds, then two of the four valence electrons on V^+ are involved in bonding. Therefore, the ground state of I must be a triplet. Based on these ideas, the correlations shown in Figure 8 can be drawn. This diagram shows an initial interaction for all states that is attractive due to the ion-dipole potential. The depth of this V^+-NH_3 well is estimated to be about the same as that for Na^+-NH_3 , 1.3 eV,⁴¹ since these ions have similar ionic radii,⁴² although the well depth could be

(39) Clemmer, D. E.; Armentrout, P. B. *J. Phys. Chem.*, submitted for publication.

(40) Steigerwald, M. L.; Goddard, W. A. *J. Am. Chem. Soc.* **1984**, *106*, 308–311. Rappe, A. K. *Organometallics* **1987**, *6*, 354–357.

(41) Castleman, A. W.; Holland, P. M.; Lindsay, D. M.; Peterson, K. I. *J. Am. Chem. Soc.* **1978**, *100*, 6039–6045.

(42) Wilson, R. G.; Brewer, G. R. *Ion Beams*; Wiley: New York, 1973.

somewhat larger.⁴³ (In all likelihood, the interaction energy is smaller for V^+ states having occupied 4s orbitals than for those which do not. In the absence of any definitive information on this effect, we use a uniform well depth for all states.) Both the a^5F and the a^3F states have repulsive surfaces at closer distances since the 4s orbital is occupied. The a^5D surface is presumably less repulsive than these states since it has a $3d^4$ configuration; but this state has the wrong spin to produce ground-state $HVNH_2^+$. Therefore, this surface also rises in energy at close interaction distances. The a^3P state (which we let represent other higher lying states as well) has both the correct spin and electron configuration to smoothly generate I. These considerations indicate that the surface evolving from a^3F crosses that evolving from a^3P . As shown in Figure 8, this surface crossing may be avoided such that a^3F could form I by mixing with the attractive surface of the a^3P or higher states. This corresponds to moving the electron originally in the 4s orbital into a 3d orbital to remove the repulsive interactions.

Now consider the spin states of the dehydrogenation products, $H_2(1^1\Sigma_g^+) + VN^+$, presumed to have a triplet ground state as noted above. Therefore, reaction of the quintet states to form VN^+ must occur via a crossing from a quintet surface to a triplet surface. Such a crossing exists, Figure 8, and presumably would require spin-orbit coupling of these surfaces. The enhanced reactivity of the triplet states is a result of favorable energy and spin, Figure 8. The relative inertness of the quintet states ($\sim 0.6\%$ as reactive as the triplet states) suggests that such spin-orbit coupling is rather inefficient in this system. Similar results were found for the reaction of V^+ with methane.¹⁶

For the endothermic production of VH^+ and VNH_2^+ , the ground states of the products are $VH^+(^4\Delta)^{22,44} + NH_2(^2A_2'')$ and $H(^2S) + VN^+$, presumed to have a quartet ground state as noted above. Thus, these reactions are spin-allowed from both quintet and triplet states of V^+ . Because of this, VH^+ and VNH_2^+ formation need not be as sensitive to the reactant state as the dehydrogenation process. However, these channels also show large magnitude increases for the triplet states (most specifically, the a^3F) reactivity compared to the quintet states. This strong state dependence for VH^+ and VNH_2^+ formation implies that the reaction proceeds predominantly through intermediate I. Note

(43) Marinelli, P. J.; Squires, R. R. *J. Am. Chem. Soc.* **1979**, *111*, 4101-4103; their results indicate that $D^0(V^+-NH_3) = 2.25$ eV.

(44) Schilling, J. B.; Goddard, W. A.; Beauchamp, J. L. *J. Am. Chem. Soc.* **1986**, *108*, 582-584; *J. Phys. Chem.* **1987**, *91*, 5616-5623. Pettersson, L. G. M.; Bauschlicher, C. W.; Langhoff, S. R.; Partridge, H. *J. Chem. Phys.* **1987**, *87*, 481-492.

that, if the critical intermediate is the simple adduct, then the potential energy surfaces of Figure 8 would predict no strong spin dependence to these reactions. The intermediacy of I, however, easily explains this dependence.

Summary

The results of this study indicate that the most likely reaction mechanism for the $V^+ + NH_3$ system proceeds via oxidative addition of a N-H bond to yield I, $H-V-NH_2^+$. Simple bond cleavage forms VH^+ and VNH_2^+ in endothermic processes, while four-center molecular elimination of H_2 leads to the exothermic formation of VN^+ . At higher kinetic energies, VNH_2^+ decomposes to form $VNH^+ + H$ and $VN^+ + H_2$.

The triplet states are found to be much more reactive than the quintet states even after accounting for differences in available energy. This is shown by the approximate state-specific cross sections shown in Figure 6. While there are sizable uncertainties in the determination of the *absolute* excited-state cross sections, the qualitative differences in reactivity are clear and unambiguous. This behavior is rationalized by using molecular orbital arguments which have been tremendously useful in understanding the reactions of atomic transition metals with H_2 and CH_4 . These lead to the qualitative potential energy surfaces for the $V^+ + ammonia$ system shown in Figure 8. These surfaces show that the triplet states can more easily form the triplet ground state of the insertion intermediate I because of spin conservation and thermochemistry. Some reactions of the quintet states of V^+ (certainly dehydrogenation, reaction 5, and any other processes evolving through the ground state of intermediate I) must involve spin-forbidden processes. These reactions presumably occur via spin-orbit mixing, which is apparently inefficient in this system as it was for the reaction of V^+ with CH_4 .

Thermochemistry for VH^+ is found to agree with previous results. New thermochemistry for VN^+ , VNH^+ , and VNH_2^+ is reported and tabulated in Table IV. Comparison of the ammonia system to analogous organic systems shows that the interaction of the lone pair electrons on the nitrogen atom with empty metal d orbitals leads to substantial increases in the bond strengths of the VNH^+ and VNH_2^+ species. Thus, these molecules have bond strengths which correspond most closely to a triple and a double bond, respectively. Also, the VN^+ bond energy implies that this molecule is triply bound.

Acknowledgment. This work is supported by the National Science Foundation, Grant No. 8796289.

Registry No. V^+ , 14782-33-3; NH_3 , 7664-41-7.

Structure, Energetics, and Vibrational Spectrum of $H_3N^+ \cdots HOH$

Zdzislaw Latajka[†] and Steve Scheiner*

Department of Chemistry and Biochemistry, Southern Illinois University, Carbondale, Illinois 62901-4409
(Received: May 23, 1989)

The geometry of $H_3N^+ \cdots HOH$ is fully optimized by using a number of basis sets including 6-31G** and variants which add a second set of d-functions and a diffuse sp-shell. The internal geometries are altered very little as a result of complexation with the exception of a 0.008-Å stretch of the bridging N-H bond; N-H \cdots O is within 5° of linearity. The electronic binding energy of the complex is 5.7 kcal/mol, 1.2 kcal/mol of which is a result of electron correlation. The calculations confirm the expected red shift and intensification of the ν_s band of the proton donor molecule within the complex. All of the intermolecular modes are calculated and used to help assign bands in the experimental spectrum.

I. Introduction

Due in part to the weakness and polar character of the hydrogen bond, its properties are sensitive to perturbation by its environment.

For this reason, recent examination of this interaction in the gas phase¹⁻⁵ and in low-temperature inert gas matrices⁶⁻⁸ has revealed

[†] Permanent address: Institute of Chemistry, University of Wrocław, F. Joliot-Curie 14, 50-383 Wrocław, Poland.

(1) Weber, A., Ed. *Structure and Dynamics of Weakly Bound Molecular Complexes*; Reidel: Dordrecht, 1987. Legon, A. C.; Millen, D. J. *Acc. Chem. Res.* **1987**, *20*, 39. Miller, R. E. *Science* **1988**, *240*, 447.